New Astronomy 21 (2013) 50–62

Contents lists available at SciVerse ScienceDirect

New Astronomy

journal homepage: www.elsevier.com/locate/newast

Snowball Earth events driven by starbursts of the Milky Way Galaxy

Ryuho Kataoka [a,*], Toshikazu Ebisuzaki [b], Hiroko Miyahara [c], Shigenori Maruyama [a]

[a] Tokyo Institute of Technology, 2-12-1-S5-4, Ookayama, Meguro-ku, Tokyo 152-8550, Japan
[b] RIKEN Advanced Science Institute, 2-1, Hirosawa, Wako, Saitama 351-0198, Japan
[c] Institute for Cosmic Ray Research, The University of Tokyo, 5-1-5 Kashiwanoha, Kashiwa, Chiba 277-8582, Japan

HIGHLIGHTS

- We present the starburst model of Snowball Earth events.
- Starburst periods of our galaxy coincide with the Snowball Earth events.
- We evaluate the effects of cosmic rays and dust particles during nebula encounters.
- Enhanced nebula encounters during the starburst can cause a Snowball Earth event.
- Direct evidence can be obtained from deep-sea sediments.

ARTICLE INFO

Article history:
Received 27 August 2012
Accepted 19 November 2012
Available online 29 November 2012
Communicated by J. Makino

Keywords:
Starburst
Snowball Earth
Supernova remnants
Dark clouds

ABSTRACT

The trigger mechanism of the Snowball Earth events at 2.2–2.4 Ga and 0.55–0.77 Ga in the Proterozoic eon remains unknown despite intensive study over the last decade. We present the starburst model of the Snowball Earth. During a starburst of the Milky Way Galaxy, frequent and prolonged encounters with dark clouds and supernova remnants occur. The increased flux of cosmic dust particles and cosmic rays during the nebula encounters lead to a global super-cool climate, a Snowball Earth event. The individual nebula encounters may correspond to the substructures of super-cool/super-warm cycles in a Snowball Earth event. The starburst periods deduced from the ages of stars and star clusters coincide well with the Snowball Earth events reconstructed from geological records. We comprehensively evaluate the effects of cosmic rays, UV radiation, and cosmic dust particles during nebula encounters for the first time, and found that the starburst model of Snowball Earth events can adequately explain the triggering and occurrence pattern of Snowball Earth events. The direct evidence of nebula encounters can be obtained from deep-sea sediments deposited during the Snowball Earth events.

© 2012 Elsevier B.V. All rights reserved.

1. Introduction

A number of geological evidences support that the Snowball Earth events occurred at 2.2–2.4 Ga and 0.55–0.77 Ga in the Proterozoic eon (Hoffman and Schrag, 2002; Maruyama and Santosh, 2008). However, previous models that included only internal forcings, e.g., the reduction of greenhouse gas in the atmosphere, had difficulty to initiate Snowball Earth events. A large negative radiative forcing equivalent to a 10% decreased solar constant, such as the reduction of $p(CO_2)$ to 0.01 mbar, was required to provide a global freezing solution. Maruyama and Liou (2005) argued that a suppression of volcanic activity might cause a significantly reduced $p(CO_2)$, driving the ice-albedo instability. Rino et al. (2008), however, found that volcanism was most active in the Proterozoic period, and thus, the atmosphere was most likely rich (by no means poor) in CO_2. Furthermore, Shaviv and Veizer (2003) found that there is no correlation between $p(CO_2)$ and ice-house and green-house climates in the last 600 Myr and suggested that external forcings cause the Earth's climate changes.

A number of previous studies have suggested that an encounter with a nebula may lead to an environmental catastrophe (Whitten et al., 1963; Ruderman, 1974; Begelman and Rees, 1976; Clark et al., 1977; Talbot and Newman, 1977; Pavlov et al., 2005a,b), which may also lead to the Snowball Earth events as follows: an encounter of the solar system with a nebula, such as dark clouds or supernova remnants, enhances the flux of cosmic dusts and cosmic rays, which leads to global cooling and destruction of the ozone layer. Pavlov et al. (2005a,b) discussed the effects on the Earth's environment during an encounter of a dark cloud. Taking into account of two shields of the Earth, *i.e.*, heliosphere and geomagnetic field of the Earth, they found that the large increase in cosmic ray flux can lead to ozone destruction and in turn mass extinctions in Phanerozoic eon (Pavlov et al., 2005b). They also

* Corresponding author. Fax: +81 3 5734 3983.
E-mail address: ryuho@geo.titech.ac.jp (R. Kataoka).

1384-1076/$ - see front matter © 2012 Elsevier B.V. All rights reserved.
http://dx.doi.org/10.1016/j.newast.2012.11.005

found that the large increase in cosmic dust flux during the encounter with a dense dark cloud can lead to a Snowball Earth event (Pavlov et al., 2005a). On the other hand, the atmospheric NO_2 also reduces the amount of insolation received at the ground (Reid et al., 1978). Furthermore, super-GeV cosmic rays produce charged ions in the troposphere that enhance aerosol nucleation (Svensmark et al., 2007), leading to greater cloud coverage and increased Earth albedo (Svensmark and Friis-Christensen, 1997; Kirkby et al., 2011). However, there has been no quantitative comparison of these several different external forcings as well as the ozone loss to explain the triggering of Snowball Earth events.

Many nebulae, including dark clouds and supernova remnants, are distributed in the galactic disk of the Milky Way Galaxy with a radius of 10 kpc and a thickness of 200 pc. A dark cloud consists of high-density (100–1000 H cm^{-3}) and low-temperature (10–100 K) neutral gas. Cosmic dust particles also exist in a dark cloud, accounting for approximately 1% of the mass of a dark cloud. The size of dark clouds ranges from 1 pc to 100 pc. In contrast, a supernova remnant is a shell structure produced by a shock wave caused by a catastrophic explosion of a star heavier than eight solar masses. Galactic cosmic rays with energies greater than 10 GeV per nucleon (the super-GeV component) are accelerated in supernova remnants. The frequency of nebula encounters in the present Milky Way Galaxy, however, is too low to explain Snowball Earth events, which require several nebula encounters in 200 Myrs: for the present Milky Way Galaxy, it has been estimated that a supernova occurs within 10 pc of the solar system, approximately once per several hundred Myr (Clark et al., 1977), whereas encountering a dense dark cloud of 2000/cc likely occurs once every billion years (Talbot and Newman, 1977).

A starburst is a phenomenon in which the star formation rate in a galaxy is, however, enhanced by dynamic interactions with nearby galaxies. A starburst galaxy, e.g., M82, is completely covered by thick, dark clouds in which numerous supernova remnants are embedded; the star formation rate and the supernova rate are significantly higher than in normal galaxies, such as the present Milky Way Galaxy. In fact, the Milky Way Galaxy is believed to have undergone several starbursts in the past. Rocha-Pinto et al. (2000) and Marcos and Marcos (2004) reconstructed the star formation rate in the past Milky Way Galaxy based on the ages of stars and star clusters and found that the Milky Way has experienced at least two starburst events, Burst I at 2.0–2.4 Ga and Burst II at 0.6–0.8 Ga, which coincide with the two known Snowball Earth events.

In such starburst periods, therefore, frequency of nebula encounters was likely to be as high as once in every several tens of Myrs, and seems possible to explain the Snowball Earth events well. Recent observations revealed that a Snowball Earth event of about a few hundred Myrs is not a simple contiguous super-cool period but is composed of several sets of super-cool periods followed by a super-warm period (Hoffman and Schrag, 2002). A super-cool/super-warm cycle may comprise a single nebula encounter.

In the present paper, we consider the ozone layer in the stratosphere as the third shield of the Earth in addition to the first shield (the heliosphere) and the second shield (geomagnetic field), and comprehensively evaluate the effects of cosmic rays, UV radiation, and cosmic dust particles, for the first time. We found that this new "starburst model of Snowball Earth events" can adequately explain the triggering and occurrence pattern of Snowball Earth events. The prolonged encounters with dark clouds and successive encounters with supernova remnants cause Snowball Earth events, which consist of several super-cool/super-warm cycles as follows: an encounter with a dark cloud shrinks the heliosphere by a factor of 100 (breakdown of the first shield) and result in the enhances of the flux of cosmic dust particles and cosmic rays, which lead to global climate cooling in the troposphere and the destruction of the ozone layer in the stratosphere (breakdown of the third shield), particularly during geomagnetic excursions (breakdown of the second shield). The duration of the encounters is from 10^4 to 10^7 yrs depending on the size of the clouds (1–100 pc) and the relative velocity (1–20 km s^{-1}) compared with the solar system. In contrast, an encounter with a supernova remnant shrinks the heliosphere (breakdown of the first shield) and also leads to a global cooling event and ozone layer destruction through enhanced cosmic rays (breakdown of the third shield). The duration of an encounter with a supernova remnant is as short as 10^4 to 10^5 yrs. A global super-cool climate and an enhanced mid-ultraviolet radiation (UV-B: 280–315 nm) due to the loss of the ozone layer may have led to mass extinction. The green-house gas accumulated in the atmosphere during the super-cool climate, resulted in a temporal super-warm period in turn after the nebula encounter was over.

The purpose of the present paper is to outline how an encounter with a nebula affects the Earth's surface environment. We further show that direct evidence of this starburst model can be found in deep-sea sediments deposited during the Snowball Earth events. It is also implicated that smaller-scale encounters with nebulae might also have led to mass extinctions in the Phanerozoic era, including the Big Five. Although the atmosphere in the Proterozoic era could be largely different from that of the present Earth, we adopt the current atmosphere of the Earth as a reference to understand how these external forcings are important because the details of the atmosphere, such as chemical composition, are not sufficiently understood. This is the first study in this direction, and the present paper will be followed by studies that are more comprehensive.

In Section 2, we describe the present situation of the Earth and introduce important factors of "three shields" (the heliosphere, geomagnetic field, and ozone layer) and "three spears" (cosmic dust particles, cosmic rays, and ultraviolet radiation). In Sections 3 and 4, we estimate the various effects of the encounters with a dense dark cloud and a supernova remnant, respectively. Based on the enhancements of the three spears and destructions of the three shields, we summarise their consequences in relation with the Snowball Earth events. In Section 5, we discuss the relation with the galactic starbursts with Snowball Earth events and the possible evidence for the model.

2. The present Earth: three shields and three spears

This section describes the situation of the present Earth. As shown in Fig. 1, three shields of the heliosphere, geomagnetic field, and ozone layer protect the Earth's environment against three spears of cosmic dust particles, sub- and super-GeV cosmic rays, and UV-B radiation from the Sun.

2.1. Three shields: the heliosphere, geomagnetic field, and ozone layer

In the present solar system, the interplanetary space is filled with the solar wind, a wind of plasma blown-off from the Sun. This area around the Sun is called as the heliosphere and controlled by the magnetic activities of the Sun. In the present solar system, the heliosphere extends across about one hundred astronomical units (1 AU = 1.5×10^8 km: a mean distance between the Sun and the Earth, Fig. 1). The outer edge of the heliosphere is determined by a balance between the dynamic pressure of the solar wind and that of outer interstellar gas. The heliosphere works as the first shield of the present Earth. The magnetic field, accumulated around the heliospheric boundary region, expels the cosmic rays with the energy under GeV and only super-GeV cosmic rays, so called galactic

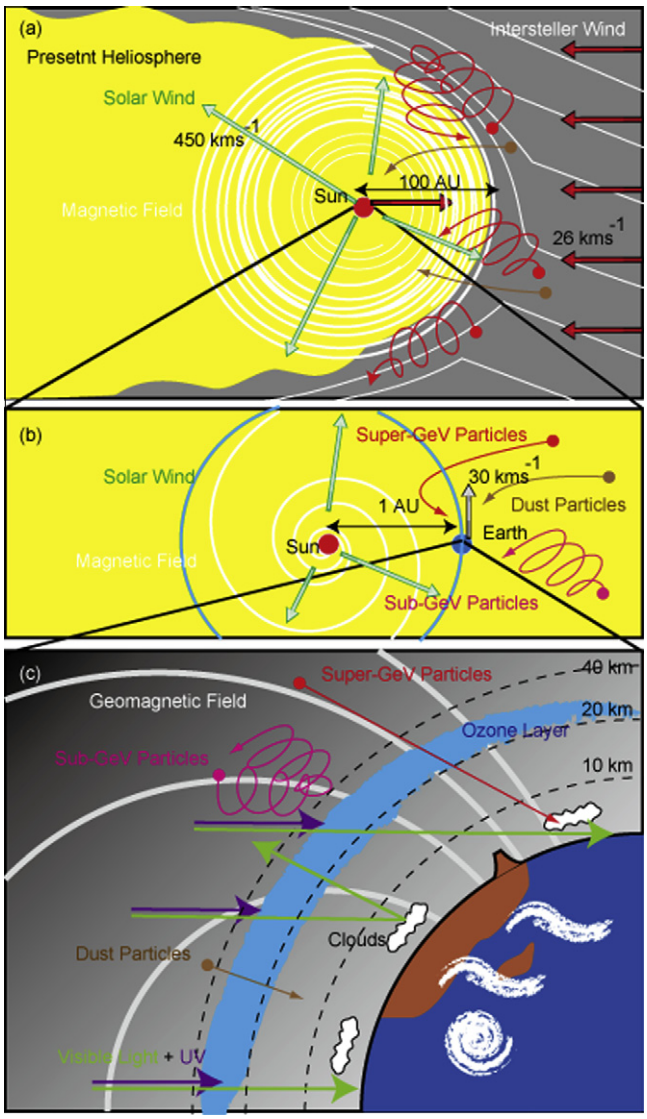

Fig. 1. Schematic picture of the present heliosphere (yellow). The solar system is travelling in the interstellar gas (grey) with relative velocity of 26 km s^{-1}. The Sun blows the solar wind to fill the heliosphere. The Earth is protected by three shields, the heliosphere, geomagnetic field, and ozone layer. First, the magnetic field of the solar wind in the heliosphere expels the cosmic rays with the energy under GeV and only super-GeV cosmic rays, so called galactic cosmic rays, penetrate into the solar system, which is modulated by the magnetic field accumulated around the heliospheric boundary. Second, geomagnetic field reflects sub-GeV cosmic rays, produced in the interplanetary space. Third, the ozone layer absorbs biologically hazardous UV-B (280–315 nm) and UV-C (100–280 nm) radiation from the Sun.

cosmic rays, penetrate into the solar system. The energy density of super-GeV cosmic rays at the Earth is kept as small as 1 eV cm^{-3}, and is modulated by the 11 yr solar cycles with the amplitude of 10–15%.

The second shield is the geomagnetic field. It blocks sub-GeV cosmic rays produced in the interplanetary space and also reduces the flux of the super-GeV cosmic rays which passes the heliosphere. Geomagnetic field is produced in the dynamo action of the Earth's core and fluctuates considerably in the time scale of several 10,000 yrs depending on the magnetohydrodynamic status there. In particular, geomagnetic field was weak, at least 10–20% of the present amplitude, during geomagnetic excursions and reversals.

The third shield is the ozone layer in the stratosphere. It absorbs biologically hazardous UV-B (280–315 nm) and UV-C (100–280 nm) radiation from the Sun in the present Earth. The increase in the sub- and super-GeV cosmic rays leads the destruction of the ozone layer in the stratosphere through the production of nitrogen oxide NO_x, which refers to NO and NO_2. NO_x formation and the subsequent ozone layer destruction in the Proterozoic atmosphere could be different from that assumed in the present work because the detailed atmospheric composition at that epoch is currently unknown. Notably, Komiya et al. (2008) found local fluctuations in the oxygen content; the peak oxygen content was as high as the current value, although the oxygen content was mostly less than 1% of PAL (present atmospheric level). Note that the overall estimation of the present study is likely to be insensitive to the O_2 levels in the Proterozoic era. Even if the Earth had a low O_2 level of 1% of PAL, Levine et al. (1979) pointed that the ozone layer still remains at lower altitude around 20 km with a similar level of ozone column density. In the present paper, therefore, we will use the present atmosphere to estimate the effects of ozone layer destruction during nebula encounters, though comprehensive studies for the Proterozoic atmosphere with differences in chemical composition must be performed in the near future.

2.2. Three spears: cosmic rays, ultraviolet radiation, and cosmic dust particles

Cosmic rays are energetic charged particles, mainly consist of protons. In this paper, we divide the cosmic rays into sub-GeV and super-GeV components depending on their energies. In the present Earth, most of the sub-GeV cosmic rays are expelled, except at the polar region, by the geomagnetic field as strong as several 10^{-5} T. The air showers produced by the sub-GeV cosmic rays stop in the stratosphere and excite the nitrogen molecule to form nitrogen oxide NO_x. The NO_x molecules work as a catalyser to destroy the ozone there through a series of chemical reactions. Furthermore, NO_2 molecules in the stratosphere have a negative radiative forcing since they absorb the visible light from the Sun (Ruderman, 1974). The air showers produced by super-GeV cosmic rays, on the other hand, reach the troposphere and ground, and deposit the energy there. In fact, the production rate of ions in the troposphere is dominated by that of super-GeV cosmic rays except just above (less than 1 km) the land. The enhancement of super-GeV cosmic rays possibly affects the Earth's environment as follows. First, it is suggested that they enhance cloud coverage of the atmosphere and then the albedo of the Earth (Svensmark, 2007), since the ions in the atmosphere lead to the increase in aerosols (Kirkby et al., 2011), which work as cloud nuclei. Second, they contribute to the radiation dose of the biological system. The energy deposition in the biological tissues can cause the double strand break of DNA molecules to lead gene duplications and shuffling (Ohno, 1970; Dubrova, 2006). Third, they may trigger eruptions of volcanoes with ferric magmas with a higher silicate content (Ebisuzaki et al., 2011).

The near ultraviolet radiation is divided into UB-A (315–400 nm), UV-B (280–315 nm), and UV-C (100–280 nm). Unlike UV-A radiation, UV-B and UV-C radiations are biologically hazardous, but are almost completely absorbed by the ozone layer in the stratosphere of the present Earth. UV-B radiation can reach the ground, only when the column density of ozone is significantly reduced, as in a case of the ozone hole, while UV-C radiation never reach there in the present Earth. UV-B and UV-C radiation cause a significant reduction of primary photosynthetic productivity in ocean. In fact, UV-B inhibits algal photosynthesis in ocean and lakes in the present Earth (e.g., Smith and Baker 1989). Although cyanobacteria, instead of eukaryotic phytoplankton, may be the major primary producers in Proterozoic period, total production by them is also likely to be suppressed under enhanced UV-B radiation.

Cosmic dust particles in the interstellar and interplanetary space are made of various solid material such as silicate, carbon (graphite or diamond), silicon carbide, or corundum. To the present Earth, cosmic dust particle fall down in a rate of about 40 million kg yr^{-1}; most of them are interplanetary dust particles produced by the collisions of the asteroids in the heliosphere, since dust particles from the outside are expelled by the magnetic field in the heliosphere boundary region, because of their electric charges. In this paper, we consider the sunshield effect of submicron particles, which stay in the stratosphere for more than several years. They scatter visible light from the Sun back into the interplanetary space. The radiative forcing by this sunshield effect is significant when the dust flux is significantly large compared to the current interplanetary dust particle (IDP) flux during the encounter with a dark cloud rich in the interstellar dust particles. It is suggested that about 100-fold enhancement of IDP flux is expected during the encounter with giant molecular clouds, and is large enough to drive the ice albedo instability (Pavlov et al., 2005a).

3. Encounter with a dark cloud

Fig. 2 depicts the interplanetary environment during a dark cloud encounter (Section 3.1). The heliospheric boundary shrinks by a factor of 100 and locates around the orbit of the Earth (breakdown of the first shield), and becomes unstable against the Rayleigh–Taylor instability, forming many cloudlets. These cloudlets orbit the Sun independently, gradually sinking down to the Sun. The shocks between these dense cloudlets and the solar wind constantly accelerate the sub-GeV component of the cosmic rays in the heliosphere (Section 3.2), unlike the present solar system, where such acceleration occurs only after intensive solar flare events. The super-GeV cosmic rays also freely penetrate the Earth's orbit (Section 3.3). The super-GeV cosmic rays enhance the radiation dose at ground (Section 3.4), and possibly cause global cooling via enhancing the cloud formation (Section 3.5). The sub-GeV cosmic rays penetrate the stratosphere of the polar region of the Earth and destroy the ozone layer through NO_x formation (breakdown of the third shield; Section 3.6), particularly during geomagnetic excursions (breakdown of the second shield). The largely enhanced NO_2 may also contribute the global cooling (Section 3.7). Furthermore, a large amount of cosmic dust particles in the dark cloud accretes on the Earth and causes global cooling (Section 3.8). Finally, we summarise their consequences in Section 3.9.

It is worth noting that the Rayleigh–Taylor (RT) instability become important only during a dark cloud encounter when the gravity is sufficiently strong to cause significant effects during passage of the fluid: when the heliosphere shrinks to 1 AU, the Kepler velocity of 30 km s^{-1} is larger than the flow speed of approximately 10 km s^{-1}, and the RT instability fully develops. On the other hand, when the heliosphere extends to 100 AU and the Kepler velocity is as low as 3 km s^{-1}, like the preset solar system, the RT instability can be ignored.

3.1. Stagnation distance

Dark clouds consist of high-density (100–1000 H cm^{-3}) and low-temperature (10–100 K) neutral gas. The size of dark clouds, R_{DC}, ranges from 1 pc to 100 pc. The duration of the encounter with a dark cloud is estimated as follows:

$$T_{DC} = 4.9\times10^{6}\ \mathrm{yr}\left(\frac{R_{DC}}{100\ \mathrm{pc}}\right)^{-1/2}\left(\frac{v_H}{20\ \mathrm{km\ s^{-1}}}\right)^{-1} \quad (1)$$

The local dynamic pressure of the neutral gas is

$$p_{DC} = 0.67\ \mathrm{nPa}\left(\frac{N_H}{1000\ \mathrm{cm^{-3}}}\right)\left(\frac{v_H}{20\ \mathrm{km\ s^{-1}}}\right)^{2}, \quad (2)$$

where N_H is the dark cloud density and v_H is the relative velocity between the dark cloud and the solar system. The neutral fluid indirectly interacts with the fully ionised solar wind plasma via charge exchange. The dynamic pressure of the solar wind is approximately 1.7 nPa at 1 AU, and the solar wind density is inversely proportional to the square of the distance, r, from the Sun:

$$p_{SW} = 1.7\ \mathrm{nPa}\left(\frac{r}{1\ \mathrm{AU}}\right)^{-2}\left(\frac{v_{SW}}{450\ \mathrm{km\ s^{-1}}}\right)\left(\frac{N_{SW}}{5\ \mathrm{cm^{-3}}}\right), \quad (3)$$

where v_{SW} and N_{SW} are the speed and density of the solar wind at 1 AU, respectively. The stagnation distance R_{stag} is determined by the pressure balance between the dark cloud and the solar wind as follows:

$$R_{stag} = 1.6\ \mathrm{AU}\left(\frac{N_H}{1000\ \mathrm{cm^{-3}}}\right)^{-1/2}\left(\frac{v_H}{20\ \mathrm{km\ s^{-1}}}\right)^{-1}. \quad (4)$$

3.2. Sub-GeV component of cosmic rays

The energy density, $p_{sub\text{-}GeV}$, of the sub-GeV component is assumed to be 20% of the total pressure of the solar wind at the stagnation distance. Following Zank and Frisch (1999), we assumed that the modulation can be described as a function of the distance of the termination shock, as approximately represented by the stagnation distance, where the simple advection–diffusion solution of the cosmic ray transport equation (Parker, 1965) gives an approximate relationship as follows:

$$p_{suv\text{-}GeV,\ ext} = \int_{0.1\ \mathrm{GeV}}^{1\ \mathrm{GeV}} E^2 N(r = 1\ \mathrm{AU}, E)\, d\ln E \ \text{and} \quad (5)$$

$$p_{sub\text{-}GeV} = \begin{cases} p_{sub\text{-}GeV,\ ext} + 0.17\ \mathrm{nJ\ m^{-3}}\left(\frac{R_{stag}}{1\ \mathrm{AU}}\right)^{-2}\exp\left(\frac{-(R_{stag}-1)}{1\ \mathrm{AU}}\right), & \text{if } R_{stag} > 1 \\ p_{sub\text{-}GeV,\ ext} + 0.17\ \mathrm{nJ\ m^{-3}}\left(\frac{R_{stag}}{1\ \mathrm{AU}}\right)^{-2}, & \text{if } R_{stag} \leqslant 1 \end{cases} \quad (6)$$

Here, we adopted a gyro radius of 0.01 AU for 100-MeV protons and a Bohm factor of 100. The dashed curve in Fig. 3 shows the enhancement of the sub-GeV cosmic rays in addition to the enhancement of the energy density of the sub-GeV component due to the modulation effect, which is calculated by assuming a current level of 0.1 eV cm^{-3} multiplied by the modulation factor at 100 MeV, as estimated from Fig. 4.

3.3. Super-GeV component of cosmic rays

The energy density, $p_{super\text{-}GeV}$, of the super-GeV component is determined by the modulation during the propagation of charged particles in the heliosphere because the super-GeV component is not produced in the heliosphere even during the encounter with a dark cloud. Cosmic rays lose their energy in the interplanetary medium as they are scattered by irregularities in the magnetic field. We used an analytical solution for the energy spectrum as follows (Gleeson and Axford, 1968):

$$\frac{N(r,E)}{E^2 - m^2} = \frac{N(\infty, E+\Phi)}{(E+\Phi)^2 - m^2} \quad (7)$$

where E is the total energy, m is the rest mass energy, $N(\infty, E)$ is the intrinsic interstellar spectrum before modulation (Usoskin et al., 2005), and Φ is the modulation parameter. We approximated the mean energy loss (Parker, 1966) of Φ as follows:

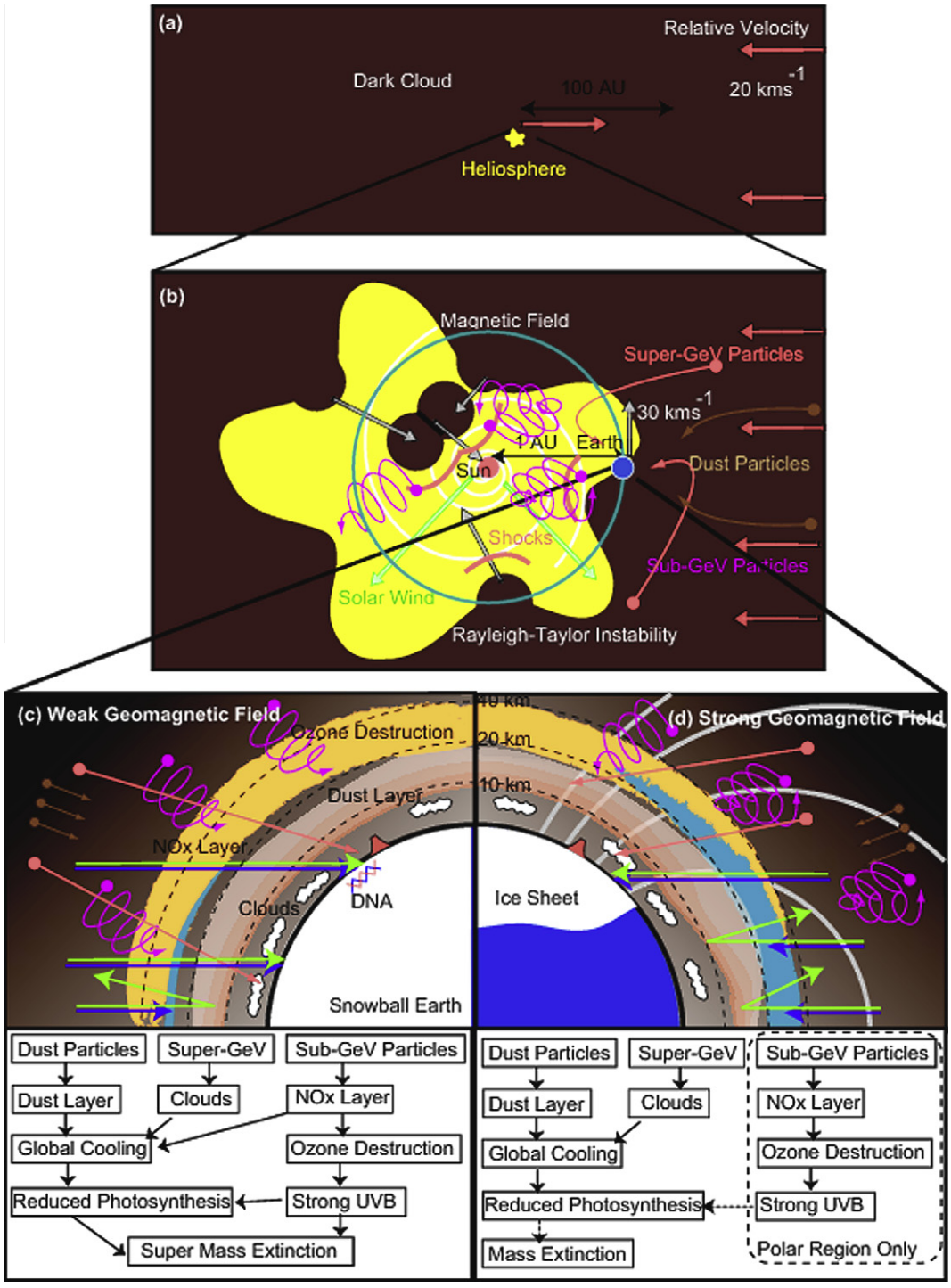

Fig. 2. Schematic pictures of the heliosphere (yellow) during an encounter with a dark cloud (brown). (a) The heliosphere shrinks to the Earth's orbit, where the enhanced ram-pressure of the interstellar gas balances that of the solar wind (breakdown of the first shield). (b) The interaction between dense cloudlets and the solar wind produces shocks and sub-GeV cosmic rays, penetrating the stratosphere of the polar region of the Earth and destroying the ozone layer through NO_x formation (breakdown of the third shield). (c) When the geomagnetic field is weak (breakdown of the second shield), such as during geomagnetic excursions or reversals, even the low latitudes are exposed to harmful UV-B radiation, leading to global destruction of the Earth's ecosystem. (d) When the geomagnetic field is as strong as that of the present Earth, the low latitude is well protected by the ozone layer from UV-B radiation.

$$\Phi = 550\ \mathrm{MeV}\left(\frac{R_{stag}}{100\ \mathrm{AU}}\right) \text{ and} \tag{8}$$

$$p_{\text{super-GeV}} = \int_{10\ \mathrm{GeV}}^{100\ \mathrm{GeV}} E^2 N(r = 1\ \mathrm{AU}, E) d\ln E. \tag{9}$$

When R_{stag} is 1 AU, the flux of the super-GeV component of the cosmic rays increases by a factor of 1.2 because of the lack of heliospheric modulation, as shown in Fig. 4. In the present paper, we ignored higher energy (>100 GeV) cosmic rays because the total energy deposition is negligible compared with lower energy cosmic rays.

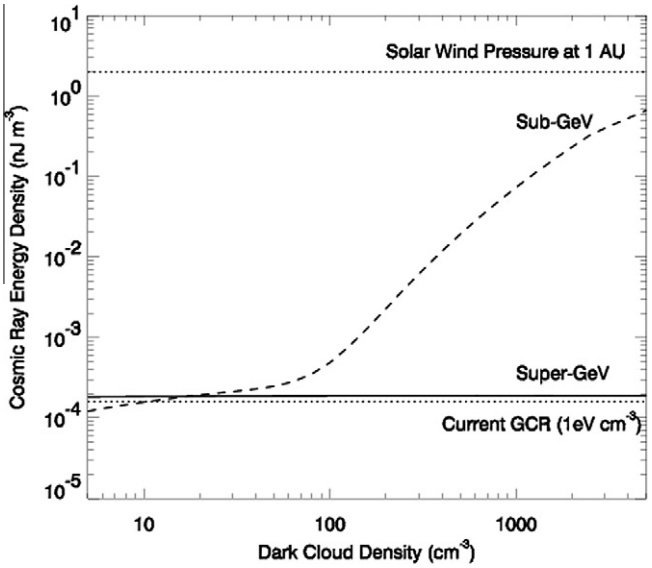

Fig. 3. Energy density of cosmic rays observed at the Earth as a function of the dark cloud density. Solid and dashed curves show the super- and sub-GeV components, respectively. The dotted line shows the current energy density of the galactic cosmic rays.

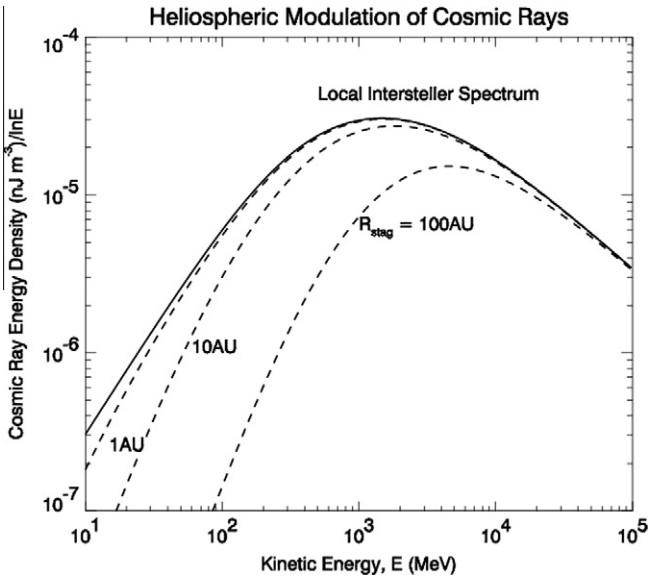

Fig. 4. Heliospheric modulation of the cosmic-ray energy-density as a function of the kinetic energy for different sizes of the heliosphere.

3.4. Dose rate of ionising radiation at the ground

The dose rate at the ground is determined by the energy density of the super-GeV component at the Earth's orbit because the super-GeV component is the main source of the air shower ionisation at ground level. In this paper, we assume that the dose rate is proportional to $p_{\text{super-GeV}}$, using the dose rate due to galactic cosmic rays of the present Earth, *i.e.*, $1\ \text{eV cm}^{-3} = 1.6 \times 10^{-4}\ \text{nPa}$ and $1\ \mu\text{Sv day}^{-1}$.

3.5. Radiative forcing by cloud formation in the troposphere

We calculated the negative radiative forcing, $\Delta F_{\text{CR-cloud}}$, due to the cloud formation associated with super-GeV cosmic rays, based on a correlation found by Svensmark (2007). Following the formulation of Shaviv (2003), we approximated the radiative forcing as follows:

$$\Delta F_{\text{CR-cloud}} = D(1 - p_{\text{GCR}}^{q})\ \text{W m}^{-2}, \tag{10}$$

where p_{GCR} is the cosmic ray energy density normalised to the present cosmic ray energy density, which is dominated by the super-GeV component. The actual values of D and q in the Proterozoic eon need to be determined in the future. In this paper, we adopted $D = 7.5$ and $q = 0.2$.

3.6. Radiative forcing by NO_2 production

The negative radiative forcing due to the NO_2 production by the sub-GeV cosmic ray enhancement is calculated based on the results of the simulation by Reid et al. (1978). They found that there are two competing factors; the increased absorption by NO_2 and the decreased absorption by the ozone layer. Considering these two factors, we calculated the radiative forcing, ΔF_{NO_2}, resulting from NO_2 production as follows:

$$\Delta F_{\text{NO}_2} = \begin{cases} 0.33 p_{\text{CR}}^{-1/3} - 1.5 \times 10^{-2} p_{\text{CR}}\ \text{W m}^{-2}, & \text{if } p_{\text{CR}} > 100 \\ 0\ \text{W m}^{-2}, & \text{if } p_{\text{CR}} \leqslant 100 \end{cases}, \tag{11}$$

where p_{CR} is the cosmic ray energy-density (the sum of the sub-GeV and super-GeV components) normalised to the present cosmic ray energy-density. The integrated radiation is negligible when $p_{\text{CR}} < 100$. When p_{CR} reaches 1000-fold, however, the increased NO_2 absorption overcomes the decreased ozone content. The integrated solar radiation is decreased as shown in Fig. 5. The concentration of O_2 at that time is currently unknown, but probably lower than the present level. This study therefore gives the upper limit of the overall NO_x effect to cool the Earth. Note that even if the NO_x effect turns out to be negligible in Proterozoic era, other factors, for example, obscuration by cosmic dust particles in the stratosphere or increased cloud amounts by super-GeV cosmic rays, can independently lead to the Snowball Earth events in nebula encounters.

3.7. Ozone layer destruction and the penetration of UV-B radiation

The sub-GeV cosmic rays penetrate into the stratosphere and deposit their energy, creating NO_x, leading to the destruction of

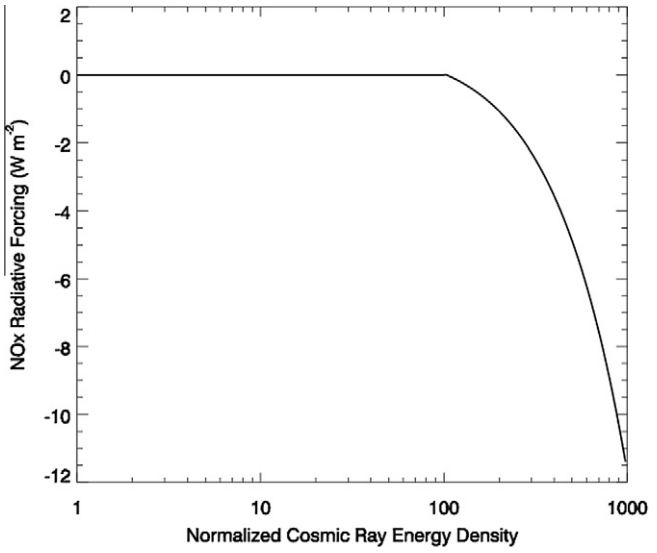

Fig. 5. Radiative forcing due to NO_2 formation in the stratosphere as a function of normalised cosmic ray energy density to the present level.

the ozone layer. This effect is more important at high-latitude regions, where the cut-off rigidity, *Rc*, is as low as 0.1 GV. Assuming a dipole-like magnetosphere, the cutoff rigidity can be formulated as follows:

$$Rc = 14.5\ \mathrm{GV}\left(\frac{1}{L^2}\right)\left(\frac{M}{M_0}\right) = 14.5\cos^4\Lambda\left(\frac{M}{M_0}\right), \tag{12}$$

where Λ is the invariant latitude derived from the McIlwain's L coordinate (McIlwain, 1961), M is the magnetic moment of the Earth at the time of the event, and M_0 is the magnetic moment at present.

Assuming cosmic rays with the theoretically hardest spectral power index (−1), the polar region higher than 75° in magnetic latitude is affected by sub-GeV cosmic rays (Fig. 6). Here, we used the results of Whitten et al. (1963), and the reduced ozone column density, Q, was approximated as a function of the normalised cosmic ray energy density, p_{CR}, as follows:

$$Q = p_{\mathrm{CR}}^{0.6} \tag{13}$$

For the encounter with a supernova remnant, Crutzen and Brühl (1996) showed ozone depletions ranging from 20% at the equator to 60% at high latitudes. This resulted in a 100-fold enhancement of the stratospheric NO_x production compared with that of the current value, using a 1D box model of the atmosphere. Conversely, Gehrels et al. (2003) performed a simulation of a 2D model and concluded that the destruction of the ozone layer is not significant if the geomagnetic field strength is as strong as in the present Earth. However, the effect of the sub-GeV cosmic rays on the ozone layer is significant during geomagnetic excursions, when the geomagnetic field is significantly weaker than that of the present Earth. For example, in the extreme case of $M = 0.01$ cosmic rays can penetrate even in latitudes lower than 20°. Furthermore, the magnetic pole tends to incline with respect to the rotation axis during magnetic excursions, which could favour a global destruction of the ozone layer.

The UV cross section in the Hartley band (200–300 nm) can be approximated as a function of the wavelength (Joens, 1994):

$$\sigma(\lambda) = 1.16\times10^{-17}\exp[-0.001614(\lambda-254)^2]\ \mathrm{cm}^2. \tag{14}$$

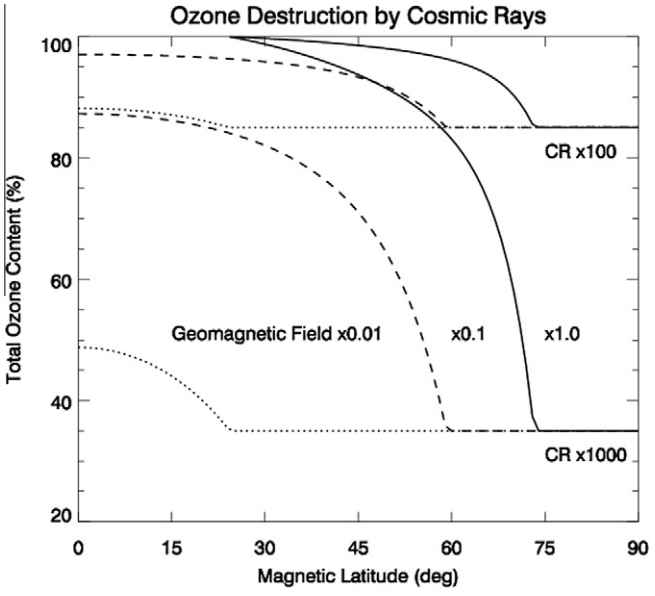

Fig. 6. Ozone destruction by cosmic rays as a function of magnetic latitude for various strengths of the geomagnetic field.

We assumed the typical column density of ozone at 60° latitude as follows:

$$N(60^\circ) = 8.1\times10^{18}\ \mathrm{cm}^{-2} = 301\ \mathrm{DU} \tag{15}$$

The UV intensity is then calculated as a function of the wavelength and the latitude as follows:

$$I_0(\lambda) = I_\infty(\lambda)e^{-\sigma(\lambda)N(x)\cos^{(-1)}x}. \tag{16}$$

The UV absorption profile in the Hartley band is shown in Fig. 7. The UV-B radiation, at wavelength less than 280 nm, is mostly absorbed by ozone in the normal state, but UV-B radiation mostly penetrates when the ozone content decreases to 10%.

3.8. Cosmic dust particles and their radiative forcing

The mass flux, f, of the extraterrestrial (or exosolar) dust particles is estimated as follows:

$$f_{\mathrm{dust}} = 1.0\times10^{-8}\ \mathrm{kg\ m^{-2}\ yr^{-1}} \times\left(\frac{N_{\mathrm{H}}}{1000/\mathrm{cc}}\right)\left[1.0\left(\frac{v_{\mathrm{H}}}{20\ \mathrm{km\ s^{-1}}}\right)+4.6\left(\frac{v_{\mathrm{H}}}{20\ \mathrm{km\ s^{-1}}}\right)^{-1}\right]^2, \tag{17}$$

where the total mass of the dust particles is assumed to be 1% of the dark cloud mass (Draine, 2011). The second term represents gravitational focussing (Begelman and Rees, 1976; Talbot and Newman, 1977). The optical thickness, τ, is estimated as follows:

$$\tau = 1.1\times10^{-2}\left(\frac{f_{\mathrm{dust}}}{3.1\times10^{-7}\ \mathrm{kg\ m^{-2}\ yr^{-1}}}\right)\left(\frac{t_{\mathrm{res}}}{10\ \mathrm{yr}}\right)\left(\frac{a_{\mathrm{dust}}}{0.2\ \mu\mathrm{m}}\right)^{-1} \times\left(\frac{\rho_{\mathrm{dust}}}{10^3\ \mathrm{kg\ m^{-3}}}\right)^{-1}, \tag{18}$$

where t_{res} is the residence time in the stratosphere, a_{dust} and ρ_{dust} are the radius and density of the cosmic dust particles, respectively. We approximated the scattering cross-section of the grains by their geometrical cross section. According to Kasten (1968), the residence time in the stratosphere is approximated as follows:

$$t_{\mathrm{res}} = 18\ \mathrm{yr}\left(\frac{a_{\mathrm{dust}}}{0.2\ \mu\mathrm{m}}\right)^{-1.3}. \tag{19}$$

Using the solar constant, $F = 1366\ \mathrm{W\ m^{-2}}$, the radiative forcing ΔF_{dust} of the cosmic dust particle is estimated as follows:

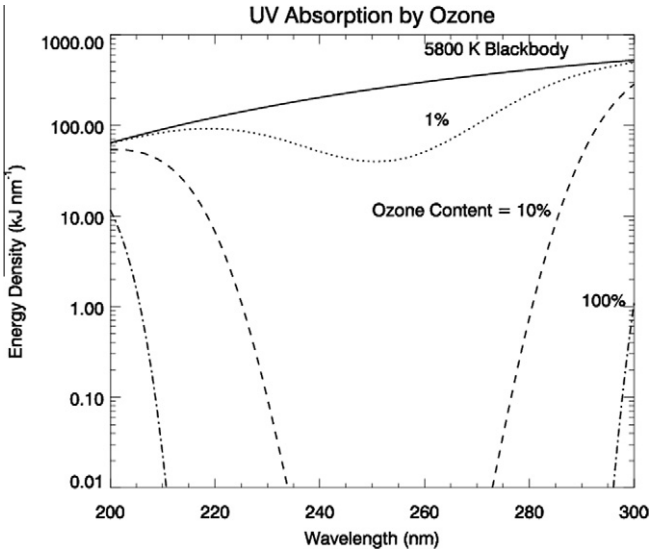

Fig. 7. UV absorption by ozone in the Hartley band.

$$\Delta F_{\rm dust} = -0.15 F\tau = -20\ {\rm W\ m^{-2}} \left(\frac{f_{\rm dust}}{3.1\times10^{-7}\ {\rm kg\ m^{-2}\ yr^{-1}}}\right) \times \left(\frac{a_{\rm d}}{0.1\ \mu{\rm m}}\right)^{-2.3} \left(\frac{\rho_{\rm d}}{10^3\ {\rm kg\ m^{-3}}}\right)^{-1}. \quad (20)$$

Here, we neglected the radiation pressure and the Poynting–Robertson drag, which are both negligible during the passage of the densest dark clouds. In fact, the results of Pavlov et al. (2005a), who evaluated solid particle flux considering the radiation pressure effect, are consistent with that found in the present work. These effects, however, may be significant for smaller particles or for less dense molecular clouds, and further study is warranted.

3.9. Consequences

Fig. 8 shows the time profiles of factors influencing the Earth's environment during an encounter with a dark cloud with a central density of 2500 H cm^{-3}, a Gaussian density profile with a scale of 10 pc across, and a relative velocity of 20 km s^{-1}. Fig. 8b shows the radiative forcings due to cosmic dust, cosmic rays, and NO_2. The most important is the effect of cosmic dust: Pavlov et al. (2005a) found that cosmic dust with submicron size particles persist in the stratosphere for several years and that the radiative forcing of cosmic dust is as large as -15 W m^{-2}, which well exceeds the snowball forcing of -14 W m^{-2} when the solar system passes the most dense part of the dark cloud. Although the atmosphere in the Proterozoic era could be largely different from that of the present Earth, it is likely to be sufficiently large to drive the Earth from an ice-free solution to a snowball solution.

The flux of the sub-GeV cosmic rays increases by a factor of approximately 1000, whereas that of super-GeV cosmic rays increases by a factor of approximately 1.2 (Fig. 8c). These increased fluxes lead to the destruction of the ozone layer in the stratosphere via the production of NO_x (in particular, NO and NO_2). Ozone depletion has been observed in the polar regions during large solar proton events (Jackman et al., 2005). The destruction of the ozone layer is limited to the polar region when the geomagnetic field is as strong as that at present time ($\sim10^{-5}$ T; Fig. 2d). The destruction, however, extends to lower latitudes during geomagnetic

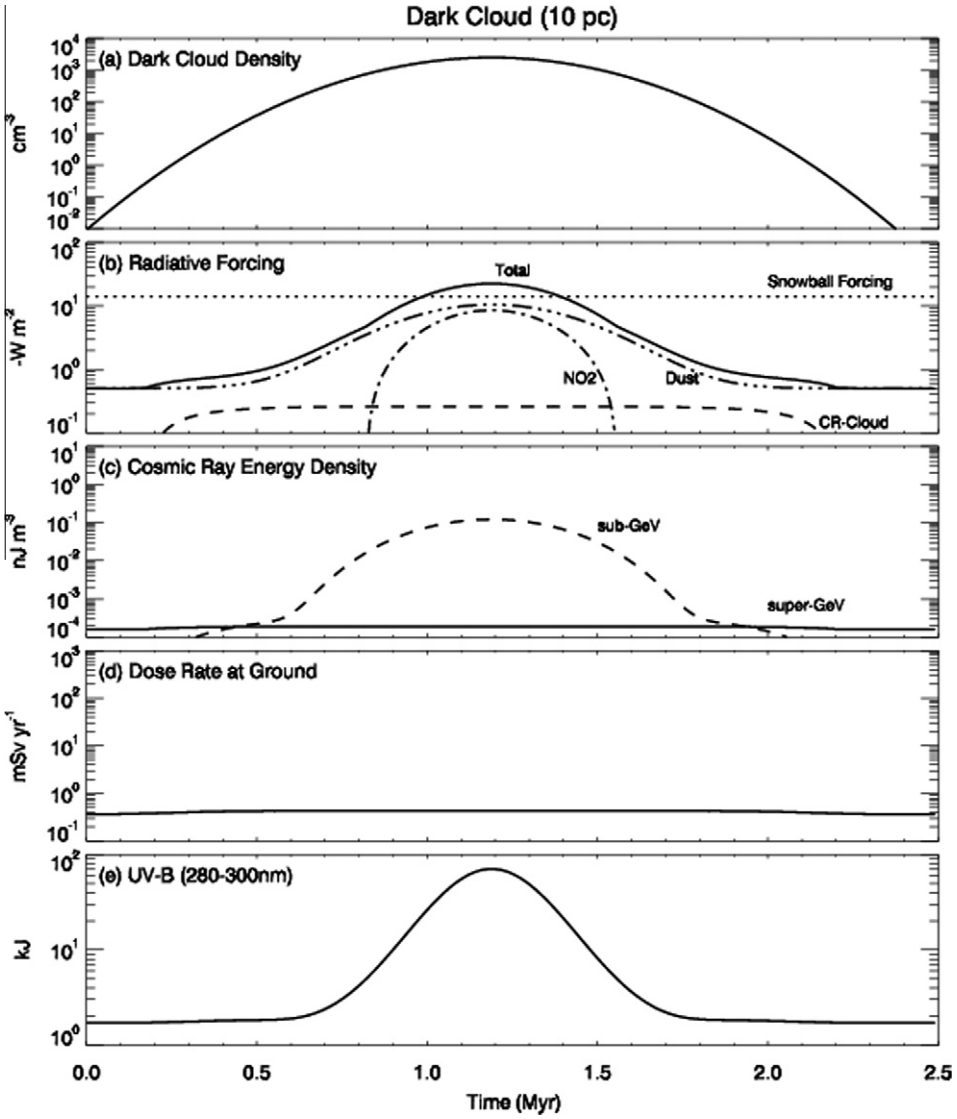

Fig. 8. Time profiles of an encounter with a dark cloud with a diameter of 10 pc and a central density of 2500 H cm^{-3}; (a) interstellar gas density; (b) negative radiative forcings (solid curve: total; dashed curve: cloud albedo by cosmic rays; dash-dot curve: NO_2 effect; dash-dot-dot curve: cosmic dust effect; and dotted line: snowball forcing of -14 W m^{-2}); (c) cosmic ray energy densities outside of the Earth's magnetosphere; (d) radiation dose rate at the ground; and (e) UV-B intensity with a weak magnetic field.

excursions when the geomagnetic field strength is low (Fig. 2c). Because at least one geomagnetic excursion or reversal is expected during a 10-Myr period (Cox, 1975), the encounter with a dark cloud, which extends for 1 Myr, is sufficiently long to encompass several geomagnetic excursions and reversals.

Fig. 8e shows the increase in UV-B radiation due to the ozone layer destruction by enhanced sub-GeV cosmic rays, assuming an ozone column density of 300 Dobson Units and a geomagnetic field as low as 10% of the present value. The UV-B radiation destroys the photosynthesis mechanisms of phytoplankton, and the primary productivity decreases to 30–50% of the present level. In fact, in the present polar ocean exposed to the enhanced UV-B flux due to the ozone hole, a reduced primary productivity of phytoplankton (Smith and Baker, 1989) has been observed. The reduced primary productivity together with the global cooling causes a reduced oxygen density in the ocean (anoxia), negative excursions of the $\delta^{13}C$, and possible mass extinction.

In addition, the accretion of cosmic dust particles may cause a large variation in the $\delta^{13}C$. Because the accreted total mass of carbon increased to $0.5 \times 10^{-7}\,\mathrm{kg\,m^{-2}\,yr^{-1}}$ and the total carbon sedimentation flux is $2.5 \times 10^{-4}\,\mathrm{kg\,m^{-2}\,yr^{-1}}$ in the deep sea, the contamination of pelagic sedimentary rocks by grains with extraordinarily high $^{13}C/^{12}C$ ratios (Amari et al., 1992), as high as 0.3, may cause high positive anomalies in the $\delta^{13}C$ of $\sim 10‰$. We therefore expect large periodic fluctuations in both the positive and negative excursions of the $\delta^{13}C$ during a nebulae encounter, as observed in the sediment around Snowball Earth events.

4. Encounter with a supernova remnant

Fig. 9 shows the interplanetary environment during an encounter with a supernova remnant. The heliosphere shrinks to the Earth's orbit (breakdown of the first shield; Section 4.1). The cosmic rays of both the super- and sub-GeV components increase by a large factor (100–1000 times; Section 4.2). The duration of the encounters are 10^4 to 10^5 yrs depending on the supernova distance and the surrounding gas density. The radiative forcings due to the increased sub-GeV and super-GeV cosmic rays is estimated as shown in the previous section, and the radiative forcing due to the cosmic dust flux is estimated in Section 4.3. The increased cosmic ray flux also depletes the ozone layer through the production of NO_x, leading to an enhanced UV-B intensity (breakdown of the third shield; Section 4.4). Finally, we summarise their consequences in Section 4.5.

4.1. Stagnation distance

During the encounter with a nearby supernova remnant, the heliosphere shrinks by a large factor. We adopted a spherically symmetric Sedov–Tayer solution (Sedov, 1946) to describe the evolution of the blast waves of a supernova. The radius, R, of the supernova shock front has a self-similar solution, $R \propto (E/n)^{1/5} t^{2/5}$, where E is the initial energy, n is the surrounding medium density, and t is the age. Following the parameters of Fields et al. (2008), we obtained an expression for the age, t, and total pressure, $p_{\rm SN}$, as follows:

$$t = 4.8\ \mathrm{kyr}\left(\frac{N_{\rm H}}{1\ \mathrm{cm^{-3}}}\right)^{-1/2}\left(\frac{R}{10\ \mathrm{pc}}\right)\left(\frac{E}{10^{51}\ \mathrm{erg}}\right)^{-1/2} \quad (21)$$

$$p_{\rm SN} = 3.3\ \mathrm{nPa}\left(\frac{R}{10\ \mathrm{pc}}\right)^{-3}\left(\frac{E}{10^{51}\ \mathrm{erg}}\right). \quad (22)$$

Here, the pressure balance between the solar wind and supernova remnant gives the stagnation distance at

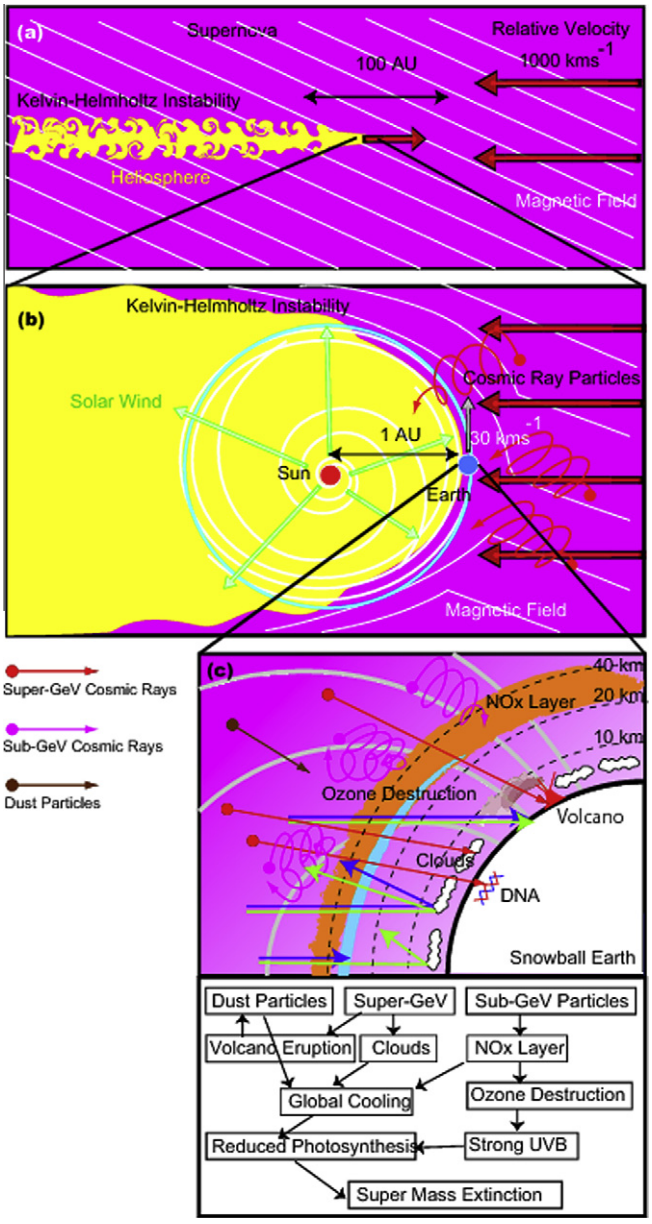

Fig. 9. Schematic pictures of the heliosphere (yellow) during an encounter with a supernova remnant (pink). (b) The heliosphere shrinks to the Earth's orbit (breakdown of the first shield), where the gas pressure of the supernova remnant balances the solar wind pressure. (c) The cosmic ray flux increases by a large factor and produces NO_x in the stratosphere, which destroys the ozone layer (destruction of the third shield); the UV-B radiation can then reach the Earth's surface. Super-GeV cosmic rays enhance cloud formation. These three factors result in a reduced photosynthesis, which leads to food and oxygen starvation in the biosphere. This starvation leads to an anoxic ocean and negative $\delta^{13}C$ excursion through biogenic CO_2 release.

$$R_{\rm stag} = 0.7\ \mathrm{AU}\left(\frac{D_{\rm SN}}{10\ \mathrm{pc}}\right)^{-3/2}, \quad (23)$$

where the $D_{\rm SN}$ is the distance of the solar system from the supernova centre.

4.2. Cosmic-ray energy density

Fig. 10 shows the time evolution of the total pressure of the supernova remnants observed at distance $R_{\rm SN}$ from the centre. As seen in Fig. 10, the total pressure of a 10-pc supernova exceeds

the solar wind pressure at the Earth's orbit. The latest measurement of the northeast shock of supernova remnant RCW 86 implied that more than 50% of the post-shocked pressure is supported by cosmic rays (Helder et al., 2009). Dashed curves show the energy density of the super-GeV component or sub-GeV component. In the present paper, we assumed that 10% and 20% of the total pressure of the post-shock layer of the supernova is converted to the energy density of the super-GeV particles and sub-GeV particles, respectively, considering the hardest spectral power index (-1). The duration of the encounter is 10^4 to 10^5 yr depending on the supernova distance, which is much shorter than for a dark cloud. The dose rate at the ground can reach 1 Sy yr^{-1} or more and continues several thousand years after the encounter with a supernova at a distance of 10 pc.

4.3. Radiative forcings

Radiative forcings due to cloud formation ($\Delta F_{\text{CR-cloud}}$) and NO_2 (ΔF_{NO_2}) are calculated as described above for the encounter with a dark cloud. The flux of cosmic dust particles is estimated as

$$f_{\text{SN}} = 1.1 \times 10^{-9}\ \text{kg m}^{-2}\ \text{yr}^{-1} \left(\frac{M_{\text{dust}}}{1.0 M_{\odot}}\right) \left(\frac{R_{\text{SN}}}{10\ \text{pc}}\right)^{-3}, \quad (24)$$

where M_{dust} is the total mass of cosmic dust particles inside of the supernova. The radiative forcing by the dust particle is then calculated as described above for the encounter with a dark cloud.

4.4. Destruction of the ozone layer and the penetration of UV-B radiation

The destruction of the ozone layer and the increased UV-B flux were calculated as described above for the encounter with a dark cloud.

4.5. Consequences

The influence of a supernova that encounters the Earth's environment is summarised in Figs. 9c and 11. First, the maximum radiative forcing due to the increased sub-GeV and super-GeV cosmic rays is approximately -20 W m^{-2} for several thousand years and well exceeds the snowball forcing of -14 W m^{-2}. Second, the dose rate at the ground reaches 1 Sy yr^{-1}, which has a significant effect on the biological systems such as genome instability (Dubrova, 2006; Nadezhda et al., 2006; Aghajanyan et al., 2011). Third, the increased cosmic ray flux depletes the ozone layer through the production of NO_x, leading to an enhanced UV-B intensity. The reduction of primary production due to this enhanced UV-B radiation, together with global cooling, causes a catastrophic turnover of the ecosystem at the surface of the Earth during a supernova encounter, similar to the effect caused by the encounter with a dark cloud.

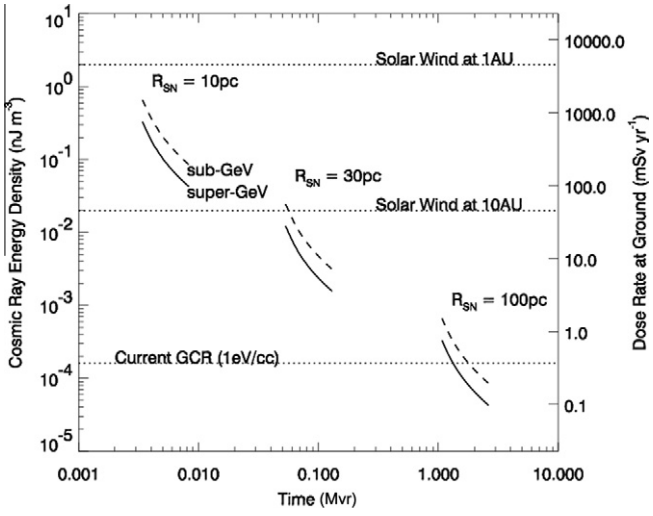

Fig. 10. Cosmic ray energy density associated with supernova blast waves (as observed at the Earth) for 10 pc, 30 pc, and 100 pc distances from the supernova centre. The corresponding dose rate at the ground is shown on the right axis.

5. Discussion

The previous Snowball Earth models, in which only internal forcings were considered, cannot explain the triggering mechanism nor occurrence pattern, while the starburst model, which includes the external forcing from the outside of the Earth, can explain both. First, the negative radiative forcing during a nebula encounter can be strong enough to trigger ice albedo instability, leading to a Snowball Earth during the solar system encounters as described above.

Second, the starburst model provides a plausible explanation for the temporal pattern of the occurrence of the Snowball Earth events that occurred only twice, during the Early Paleoproterozoic era (around 2.3 Ga) and the Late Neoproterozoic period (0.8–0.6 Ga) (Fig. 12b). Based on the statistics of stars and star clusters, this implies that the Milky Way Galaxy has experienced at least two starburst events (Burst I: 2.0–2.4 Ga; Burst II: 0.6–0.8 Ga), as shown in Fig. 12a. Bursts I and II correspond to the Snowball Earth events in the Early Paleoproterozoic era and the Late Neoproterozoic era, respectively. According to Marcos and Marcos (2004), the error in the age estimation of the star clusters is likely 50–150 Myr for the youngest cluster (age < 0.5 Gyr) and 150–250 Myr for the older cluster. These numbers are small in comparison with the geological age of the Snowball Earth events. Kono and Tanaka (1995) emphasised that the geomagnetic field is approximately 25% of the current strength and the quadrupole component dominated in Late Neoproterozoic era. The weak geomagnetic field may be one reason why Snowball Earth events in the Late Neoproterozoic era were as severe as those that occurred in the Early Paleoproterozoic era, though Burst II was less intense than Burst I.

The maximum encountering rate of nebula encounter during the starburst is estimated to be several events in 200 Myrs to explain the geological record, which is an order of magnitude larger rate than that of the present Milky Way Galaxy. One must be very careful to compare the amplitudes of the fluctuations in different periods in Fig. 12a. Note that the situation is much better in the ages, which have the firm basis of the theory of the stellar evolution. We used the star formation rate without correction of selection effect in Fig. 12a, since it is dangerously difficult. If we take into account of the effects of the selection, the Burst II must be more prominent probably at least by a factor of 10 than those in Phanerozoic era, which are probably related to the mass extinction events, like Big Five.

In the Late Neoproterozoic era, two Snowball Earth events occurred (Sturtian and Marinoan), separated by 100 Myrs. Recent observations revealed that a Snowball Earth event is not a simple contiguous super-cool period but is composed of several sets of super-cool periods followed by a super-warm period (Hoffman and Schrag, 2002). Such a hierarchical temporal structure in geological records of Snowball Earth events may correspond to the hierarchical nature of the galactic disk; in other words, from the entire disk, through spiral/bar structures, to individual nebulae. During a starburst, the negative radiative forcing due to cosmic dust particles kept high for a several hundred Myrs, since the entire

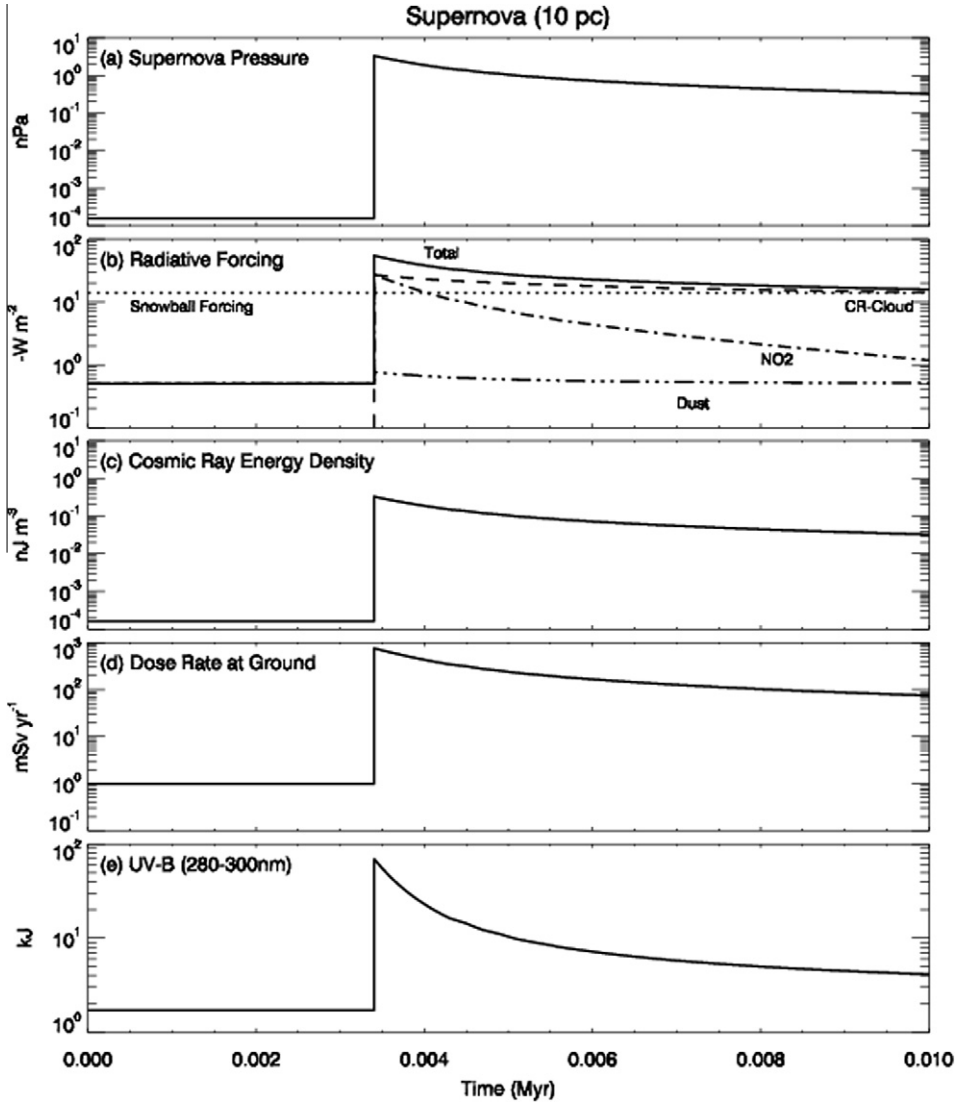

Fig. 11. Time profiles of the encounter with a supernova remnant that exploded at a distance of 10 pc and with an interstellar gas density of 0.5 H cm^{-3}: (a) pressure of the post-shocked gas of the supernova remnant; (b) negative radiative forcings (solid curve: total; dashed curve: cloud albedo by cosmic rays; dash-dot curve: NO_2 effect; dash-dot-dot curve: cosmic dust effect; and dotted line: snowball forcing of -14 W m^{-2}); (c) cosmic ray energy density; (d) radiation dose rate at the ground; and (e) UV-B intensity.

galactic disk is almost covered by relatively thin dark cloud (10–100 H cm^{-3}) as shown in Fig. 12d. When the solar system encountered the dense cores ($\sim$1000 H cm^{-3}) of dark clouds and supernova remnants, which are embedded into the thin dark cloud, super-cool climates took place. A super-cool/super-warm cycle in the Snowball Earth periods may comprise a single encounter with dense core of dark cloud or a supernova remnant (Fig. 12e): after the super-cool period is triggered by a nebula encounter, the climate becomes super-warm because of the accumulation of CO_2 in the atmosphere because of reduced photosynthesis. Note also that a Snowball Earth event that continues for approximately 50 Myr can be explained by a starburst with a typical duration of 100 Myr but not by a spiral arm passing that lasts approximately 10 Myr.

The starburst model is a working hypothesis. Evidence to support the model may be provided by detailed geochemical studies, including isotope studies of platinum-group elements or plutonium in deep-sea sediments where the accumulation speed is sufficiently low. These types of studies may predict the existence of a large amount of exosolar grains in the sediment during the Snowball Earth period. As a possible evidence of very recent supernova, an excess of ^{60}Fe has been observed in a Fe/Mn crust in marine sediments (Knie et al., 2004; Fields et al., 2005). This excess was interpreted as a signature of a supernova explosion 2.8 ± 0.4 Myr ago.

Bodiselitsch et al. (2005) found iridium anomalies at the base of all cap carbonates both after the Marinoan and Sturtian glaciations. Iridium and other platinum-group elements are typical proxies for extraterrestrial (including exosolar) materials and are much more abundant than in the Earth's upper mantle and crust. The authors interpreted these anomalies as the product of the rapid accumulation of extraterrestrial material that was once trapped in surface ice and later transported to the ocean floor via the melting of the ice at the end of the glaciation. Nevertheless, the excursion of iridium may also reflect the enhanced flux of extraterrestrial material due to an encounter with a nebula.

Moreover, ^{244}Pu is expected to remain in the Fe/Mn crusts of interest. Fields et al. (2005) estimated the ^{244}Pu production by a supernova explosion to approximately 0.9×10^{-7} solar masses. The expected flux of the ^{244}Pu at the Earth is approximately 10^{-16} kg m^{-2} yr^{-1}. A significant amount (0.1 Bq m^{-2}) of the accreted ^{244}Pu remains in the sedimentary rocks, even considering the half-life of ^{244}Pu (80 Myr).

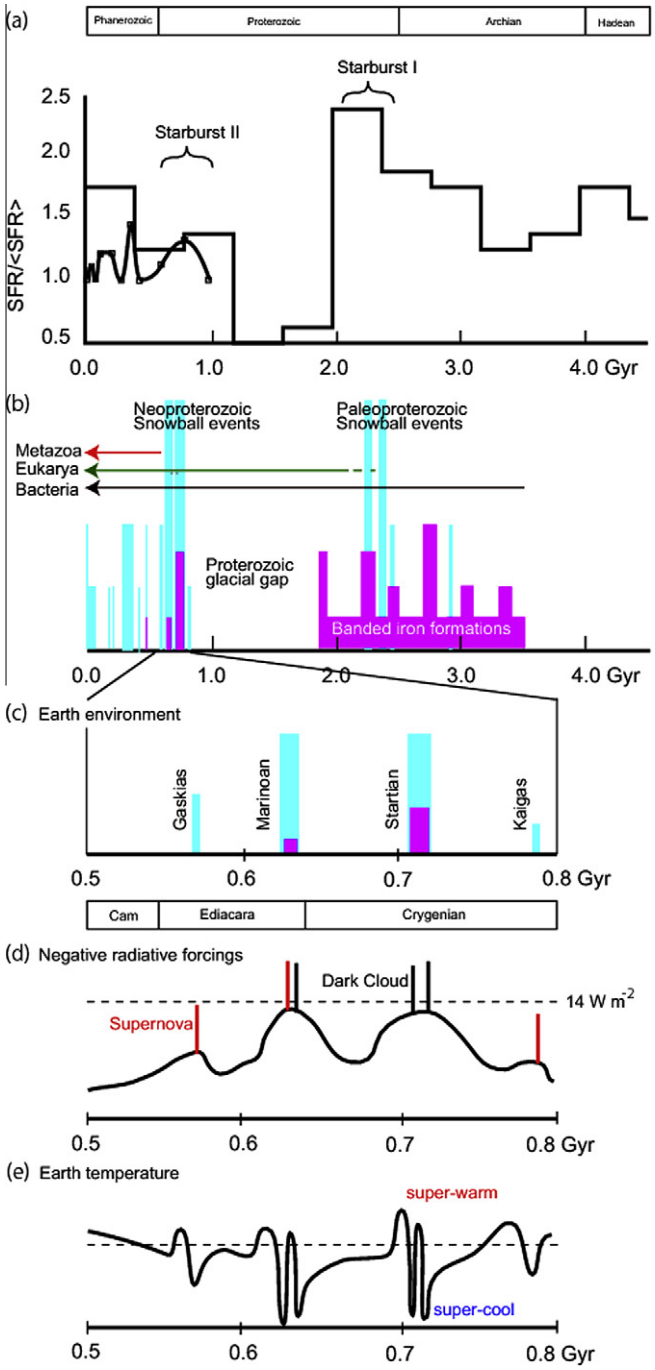

Fig. 12. Star formation rate in the Milky Way Galaxy and during Snowball Earth events: (a) two major starburst events were observed in the history of the star formation rate by Rocha-Pinto et al. (2000) and Marcos and Marcos (2004). Note that the age bias is still prominent, and a direct comparison between the intensity of bursts during different epochs is difficult. (b) There are two Snowball Earth events at similar time intervals of starburst periods that well coincide with Burst II (0.6–0.8 Ga) and are separated by 100 Myr^{24}, consistent with the typical duration of a starburst. (c) Earth environment during the Neoproterozoic Snowball Earth event. (d) Schematic drawing of the variation of the radiative forcing during Burst II due to encounters with dark clouds or supernovae. (e) Schematic drawings of the variation of the temperature of the Earth during Burst II.

The existence of abundant spherule particles, 100-μm spherical iron balls, in the sediment is also possible direct evidence. For example, Miono et al. (1993) argued that the spherules accumulate in Paleozoic–Mesozoic bedded cherts. These spherules are generally believed to originate from micro-meteorites.

The cosmic ray-cloud connection is not firmly established and controversial (see Yu et al., 2008 and their discussion for details) in the present atmosphere of the Earth. For example, Erlykin and Wolfendale (2011) recently concluded that cosmic rays have negligible effect on climate. However, the majority of the averaged data of ISCCP and some others used in their analysis do not necessary give the true upper limit and possibly miss the important fundamental processes. More careful examination of the cloud properties with fine temporal and spatial resolutions is needed and important to reveal and evaluate the potential effect of cosmic rays in a long term with possible large amplitude variation as proposed in this study. For example, note that Svensmark et al. (2012) recently conducted more detailed analysis during Forbush events to examine the possible effect of cosmic rays on cloud properties. Apart from the present atmosphere, in the past, it is likely to exercise a climate effect due to the enhanced ionisation rate by a large factor (100–1000) in the troposphere through super-GeV cosmic rays because of encounters with supernova remnants and dark nebulae: two independent experiments clearly showed significant increases in the formation of cloud condensation nuclei by enhanced ionisation rate in the atmosphere (Svensmark et al., 2007; Kirkby et al., 2011).

Overholt et al. (2009) cast doubt on the correlation between ice houses and the spiral arm pattern of our Galaxy, assuming the current CO data and the fixed spiral pattern. This assumption, however, is unlikely to be valid: the recent precise simulations of the Milky Way Galaxy suggested the spiral pattern itself is quite unstable (Baba et al., 2010), and so as the period of encounters to them. Furthermore, environment of galaxy drastically changed in the past, in particular, two starbursts with enhanced star formation rates by at least several times are suggested in Proterozoic era (Rocha-Pinto et al., 2000; Marcos and Marcos, 2004), as we discussed in the present paper. Much more careful comparisons between Earth's climate records and galaxy environment have to be done in near future, though it is beyond of the scope of the present paper.

A mass extinction, such as the Big Five, may be related to a similar but a smaller-scale encounter with a dark cloud or a supernova remnant during the Phanerozoic eon (542 Ma to present). The encounters with a combination of minor dark clouds and supernovae may cause mass extinction events at the P–T boundary as well as other geological boundaries. In fact, Baba et al. (2012, private communication) performed a series of N-body simulations and succeeded in reproducing realistic behaviours observed in the present (normal or non-starburst) state of the Milky Way Galaxy. They found an encounter frequency of 100 $Myrs^{-1}$ with dark clouds or supernova remnants. They also found significant fluctuations in the encounter frequency that may correspond to the ice-house of the Earth in the Phanerozoic eon. Their results are consistent with our results. It may also be worth reconsidering the cause of the extinction at the K–T boundary. This extinction is currently explained by the collision with an asteroid (Alvarez et al., 1980); however, this extinction may alternatively be related to a nebula encounter.

Finally, an increase (by a factor of 100–1000) in the radiation dose rate at the ground leads to genome instability (Dubrova, 2006), which may accelerate the evolution of life through segmental or whole-genome duplication (Ohno, 1970) and induce gene shuffling. The dose rate of cosmic ray irradiation during nebulae encounters reaches 1 Sy yr^{-1} and possibly contributes to the explosive emergence of new types of animals after mass extinctions.

Acknowledgements

We acknowledge interdisciplinary discussions with the Interactive Research Center of Science, Tokyo Tech. To understand this

interdisciplinary field at the interface of geology, biology, and astrophysics, we read numerous papers. We express sincere thanks to all the efforts of the librarians in Japan, who supplied us with copies of papers through the Interlibrary Copy Order Service. We also thank Prof. Gustavo Medina-Tanco, who read our manuscript and provided useful suggestions. This work was supported by Grants-in-Aid for Scientific Research (23224012) from the Japanese Ministry of Education, Science, Sports, Technology, and Culture.

References

Aghajanyan, A. et al., 2011. Envirom. Mol. Mutagen. 52, 538.
Alvarez, L.W. et al., 1980. Science 208, 1095.
Amari, S., Hoppe, P., Zinner, E., Lewis, R.S., 1992. Astrophys. J. 394, L43.
Baba, J., Saitoh, T.R., Wada, K., 2010. Publ. Astron. Soc. Jpn. 62 (6), 1413.
Begelman, M.C., Rees, M.J., 1976. Nature 261, 298.
Bodiselitsch, B., Koeberl, C., Master, S., Reimold, W.U., 2005. Science 308, 239.
Clark, D.H., McCrea, W.H., Stephenson, F.R., 1977. Nature 265, 318.
Cox, A., 1975. Rev. Geophys. Space Phys. 13, 3.
Crutzen, P.J., Brühl, C., 1996. Proc. Natl. Acad. Sci. U. S. A. 93, 1582.
Draine, B.T., 2011. Physics of the Interstellar and Intergalactic Medium. Princeton University Press, p. 246.
Dubrova, Y.E., 2006. Russ. J. Genet. 42, 1116.
Ebisuzaki, T., Miyahara, H., Kataoka, R., Sato, T., Ishimine, Y., 2011. Gondwana Res. 19 (4), 1054.
Erlykin, A.D., Wolfendale, A.W., 2011. J. Atmos. Sol. Terr. Phys. 73 (13), 1681.
Fields, B.D., Hochmuth, K.A., Ellis, J., 2005. Astrophys. J. 621, 902.
Fields, B.D., Athanassiadou, T., Johnson, S.R., 2008. Astrophys. J. 678, 549.
Gehrels, N. et al., 2003. Astrophys. J. 585, 1169.
Gleeson, L.J., Axford, W.I., 1968. Astrophys. J. 154, 1011.
Helder, E.A. et al., 2009. Science 325, 719.
Hoffman, P.F., Schrag, D.P., 2002. Terra Nova 14, 129.
Jackman, C.H. et al., 2005. J. Geophys. Res. 110, A09S27.
Joens, J.A., 1994. J. Chem. Phys. 100 (5), 3407.
Kasten, F., 1968. J. Appl. Meteorol. 7, 944.
Kirkby, J. et al., 2011. Nature 476, 429.
Knie, K. et al., 2004. Phys. Rev. Lett. 93, 17.
Komiya, T. et al., 2008. Gondwana Res. 14, 159.
Kono, M., Tanaka, H., 1995. In: Yukutake, T. (Ed.), The Earth's Central Part: Its Structure and Dynamics. Terra Scientific Publishing Company, p. 75.
Levine, J.S., Hays, P.B., Walker, J.C.G., 1979. Icarus 39, 295.
Marcos, R., Marcos, C., 2004. New Astron. 10, 53.
Maruyama, S., Liou, J.G., 2005. Int. Geol. Rev. 47 (8), 775.
Maruyama, S., Santosh, M., 2008. Gondwana Res. 14, 22.
McIlwain, C.E., 1961. J. Geophys. Res. 66 (11), 3681. http://dx.doi.org/10.1029/JZ066i011p03681.
Miono, S., Nakayama, Y., Shoji, M., Tsuji, H., Nakanishi, A., 1993. Nucl. Instrum. Methods Phys. Res. B75, 435.
Nadezhda, I., Ryabokon, R., Goncharova, I., 2006. Radiat. Environ. Bioph. 45, 167.
Ohno, S., 1970. Evolution by Gene Duplication. Springer-Verlag, Berlin.
Overholt, A.C., Melott, A.L., Pohl, M., 2009. Astrophys. J. 705, L101. http://dx.doi.org/10.1088/0004-637X/705/2/L101.
Parker, E.N., 1965. Planet. Space Sci. 13, 9.
Parker, E.N., 1966. Planet. Space Sci. 14, 371.
Pavlov, A.A., Toon, O.B., Pavlov, A.K., Bally, J., Pollard, D., 2005a. Geophys. Res. Lett. 32, L03705.
Pavlov, A.A., Pavlov, A.K., Mills, M.J., Ostryakov, V.M., Vasilyev, G.I., Toon, O.B., 2005b. Geophys. Res. Lett. 32, L01815. doi: 10.1029/2004GL021601.
Reid, G.C., McAfee, J.R., Crutzen, R.J., 1978. Nature 275, 489.
Rino, S. et al., 2008. Gondwana Res. 14 (1–2), 51.
Rocha-Pinto, H.J., Scalo, J., Maciel, W.J., Flynn, C., 2000. Astron. Astrophys. 358, 869.
Ruderman, M.A., 1974. Science 184, 1079.
Sedov, L.I., 1946. J. Appl. Math. Mech. 10, 241.
Shaviv, N.J., 2003. J. Geophys. Res. 108 (A12), 1437. doi: 10.1029/2003JA009997.
Shaviv, N., Veizer, J., 2003. GSA Today 13, 4.
Smith, R.C., Baker, K.S., 1989. Oceanography 20, 4.
Svensmark, H., 2007. Astron. Geophys. 48 (1), 1.18.
Svensmark, H. et al., 2007. Proc. R. Soc. A 463, 385.
Svensmark, H., Friis-Christensen, E., 1997. J. Atmos. Sol. Terr. Phys. 59, 1225.
Svensmark, J., Enghoff, M.B., Svensmark, H., 2012. Atmos. Chem. Phys. Discuss. 12, 3595.
Talbot, R.J., Newman, M., 1977. Astrophys. J. Suppl. Ser. 34, 295.
Usoskin, I.G., Alanko-Huotari, K., Kovaltsov, G.A., Mursula, K., 2005. J. Geophys. Res. 110, A12108. doi: 10.1029/2005JA011250.
Whitten, R.C., Cuzzi, J., Borucki, W.J., Wolfe, J.H., 1963. Nature 263, 398.
Yu, F. et al., 2008. Atmos. Chem. Phys. 8, 2537.
Zank, G.P., Frisch, P.C., 1999. Astrophys. J. 518, 965.